Electronic Supplementary Information (ESI)

Rectangular ZnO porous nano-plate assembly with excellent acetone sensing performance and catalytic activity

Arnab Kanti Giri, [a] *Arka Saha,* [a] *Aniruddha Mandal,* [a] *Subhash Chandra Ghosh,* [a] *Susmita Kundu,* [b] *Asit Baran Panda* [a]

[a] Discipline of Inorganic Materials and Catalysis and Academy of Scientific and Innovative Research, CSIR-Central Salt and Marine Chemicals Research Institute, G.B. Marg, Bhavnagar-364002, Gujarat, India.

[b] Sensors and Actuators division, CSIR-Central Glass & Ceramic Research Institute, Kolkata-700032, West Bengal, India.

Email: abpanda@csmcri.org, Tel: + 91-2782567040. Fax: + 91-2782567562

Details of the preparation of 0.5-1 ppm acetone through serial dilution method

A certain concentration of acetone vapour $C1_{ppm}$ was prepared by adding a required amount of liquid (V_1 in ml) acetone using a micropipette in a desiccator using the equn. (1) [1-2]

$$V_1 = \frac{C1_{ppm} \times Va \times M}{24.5 \times 10^9 \times D} \qquad (1)$$

Va = Volume of 1st the desiccator in ml

M = Molecular weight of acetone in gm

D = Density of acetone in gm/ml

Then the vapour was homogenised using a small mechanical fan. Afterwards the required lower concentration $C2_{ppm}$ was prepared by serial dilution using the equn. (2)

$$C2_{ppm} \times V_b = C1_{ppm} \times V_2 \qquad (2)$$

V_2 = Volume of the required acetone vapour in ml

V_b = Volume of the 2nd desiccator in ml

Diagram of the "*Gas Sensing Experiment*":

A voltage/current source (Keithley 228A) was connected with two terminals linked with the heating coils of the sensor (Fig. S1) from which the heat was generated. The operating temperature we measured from the voltage given in power source which was pre-calibrated at our measurement condition (Fig.S1). We also used FLUKE make thermal imager (Model Ti32) to know the sample temperature where the temperature varied within ±5°C. We have made 5 sensors to check the reproducibility of the data.

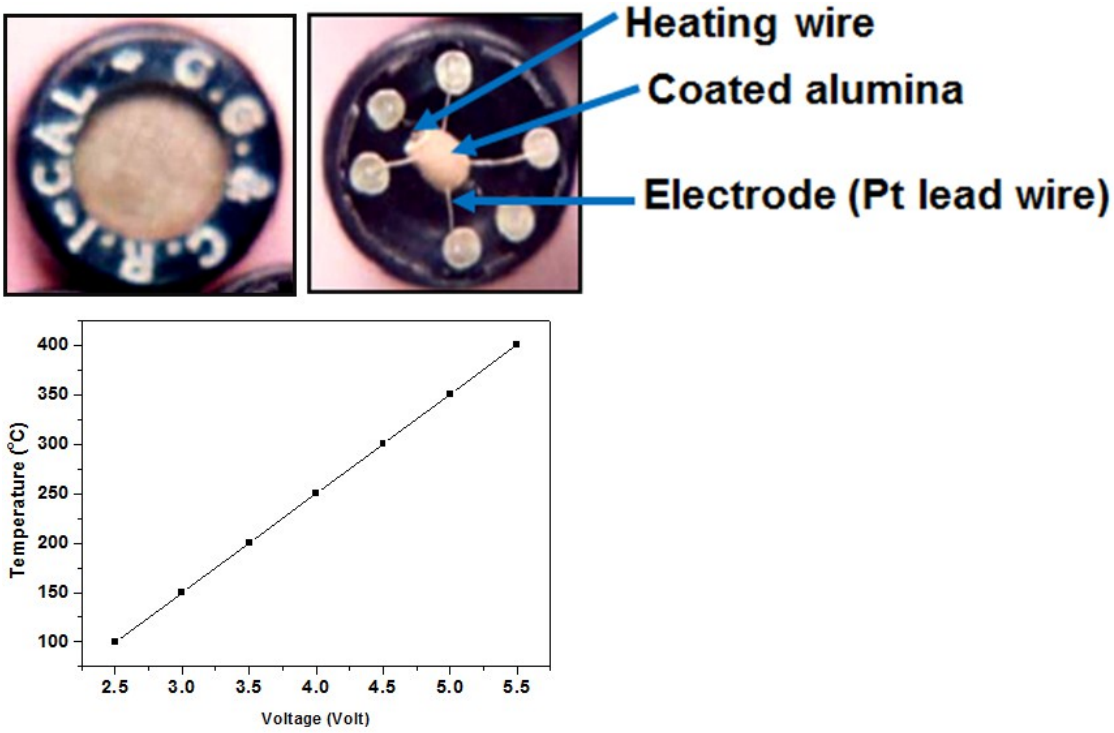

Fig S1. Outer view, inner view of fabricated sensor and corresponding Voltage-Temperature calibration curve.

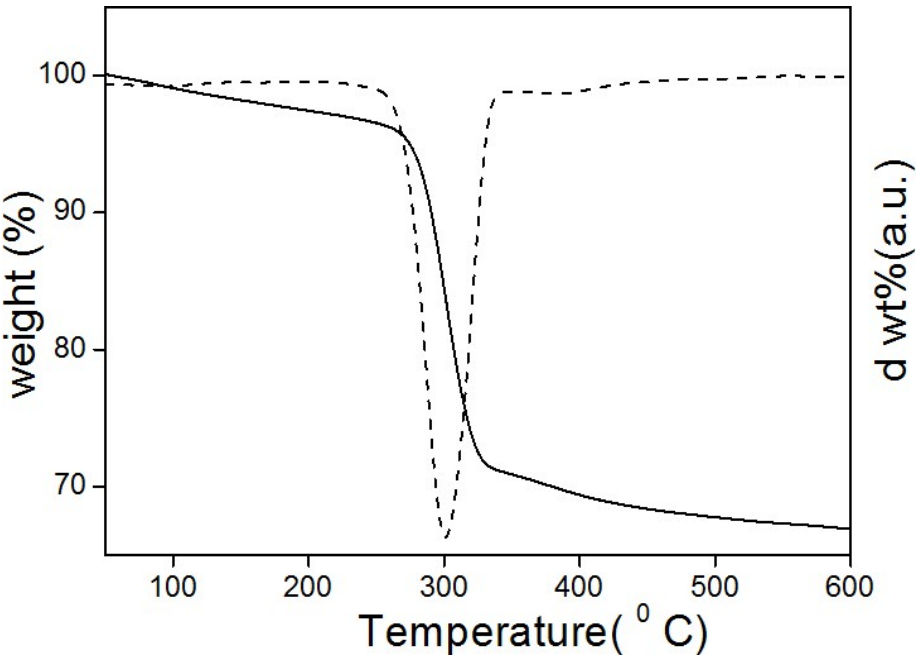

Fig. S2 TG-DTG curve of hydrozincite intermediate.

In the TG and DTG curves of the synthesized hydrozincite under air flow the initial weight loss (~5%) in the temperature range of 30 -250°C can be assigned to the removal of adsorbed water, trapped carbon dioxide and ammonia and the weight loss in second stage (27.5%) the temperature range of 200–475°C is correspond to the removal of H_2O and CO_2 due to the decomposition of hydrozincite to ZnO. No distinct weight loss after 475 °C indicates the total decomposition of hydrozincite intermediate and the 27.5 % weight loss in second stage is very close to that of theoretical weight loss (26.2%) of hydrozincite and confirmed that intermediate is nothing but hydrozincite.

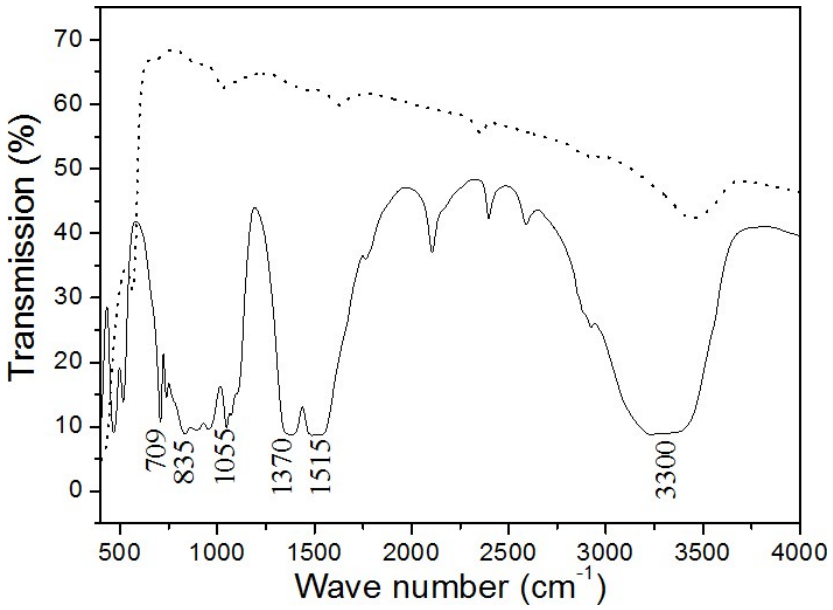

Fig. S3. FT-IR spectra of hydrozincite intermediate (solid) and ZnO calcined at 500°C for 2h (dot).

Further, in the FT-IR spectrum of carbonate intermediate, the sharp bands at 708, 832, 1386, 1506 cm^{-1} are the the characteristic bands for the C-O bending vibration of CO_3^{2-}. The broad band at 3298 cm^{-1} is due to the hydroxyl group and adsorbed water molecule. On calcination (at 500°C/2h), the bands corresponding to C-O and hydroxyl groups /water molecules were almost diminished and confirmed the conversion to ZnO. The bands for

respective C-O and hydroxyl/water with low intensity in the calcined materials are probably due to the surface adsorbed CO_2 and water.

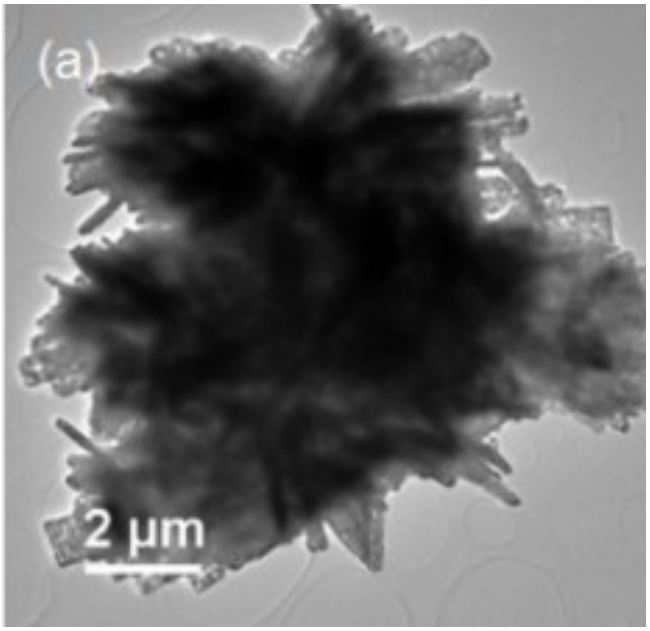

Fig. S4 TEM images of synthesized Porous Rectangular ZnO nanopalte architecture calcined at 500°C depicting the 3D assembly of the plates.

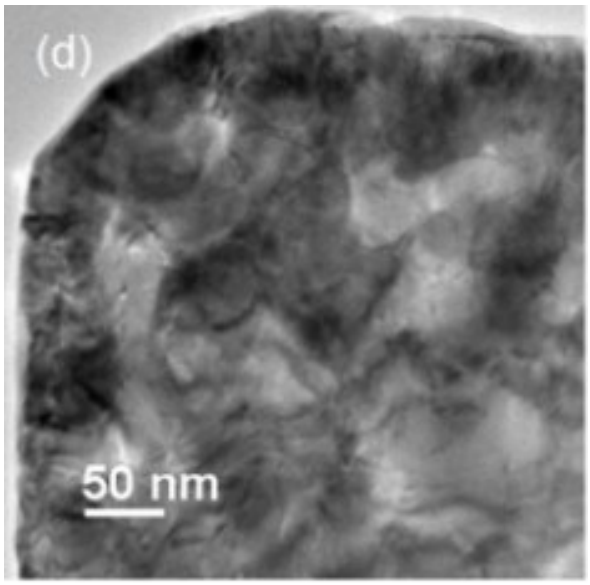

Fig. S5 TEM images of synthesized porous rectangular ZnO nanopalte architecture calcined at 500°C showing the porous structure in the surface of the plates.

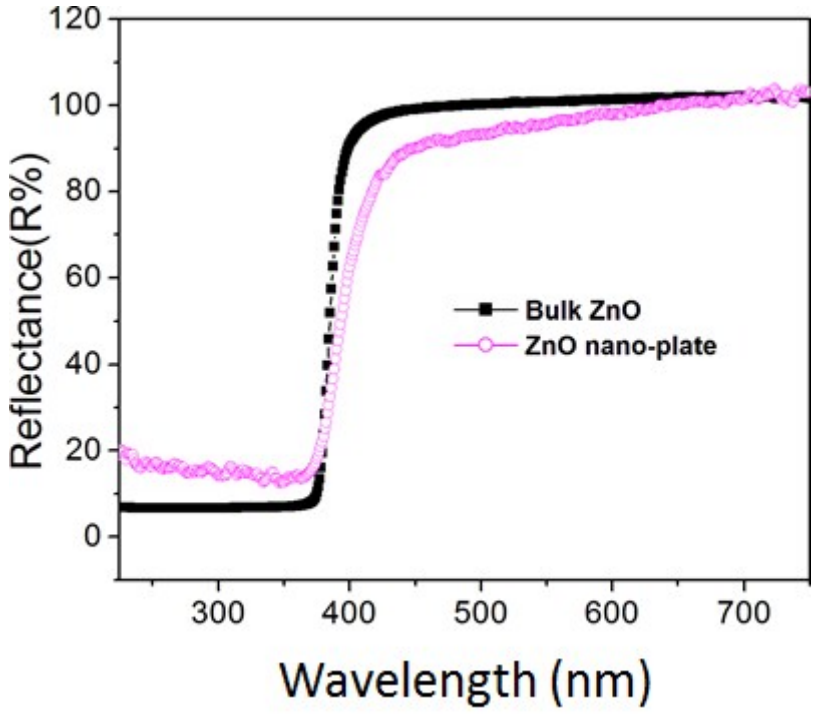

Fig. S6 DRS spectra of the synthesized ZnO nanoarchitecture calcined at 500°C and bulk ZnO.

ZnO is frequently used as a UV filter, thus DRS spectroscopic measurement of the synthesized 3d assembled ZnO architecture was also performed. Fig. S6 represents the DRS spectra of synthesized ZnO calcined at varying temperatures as well as bulk ZnO for comparison. All the ZnO samples including bulk ZnO showed almost identical spectra but for the synthesized ZnO architectures very little shifting of band edge towards blue reason with respect to corresponding bulk was observed. However, this minute shifting is unusual as the particle size of the synthesized ZnO is quite high than that of its Bohr radius. This is most probably due to the presence of very thin bridge between the synthesized nanoparticles.

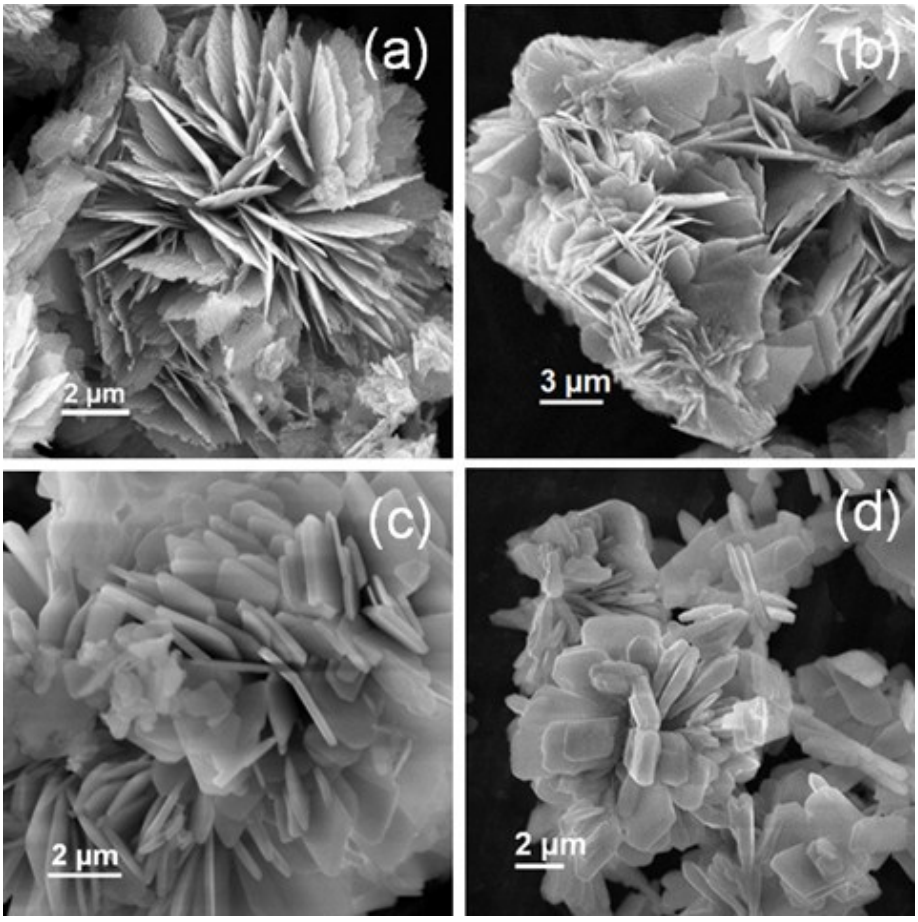

Fig. S7 SEM images of hydrozincite intermediates formed after 24h of hydrothermal treatment in varying temperature, (a) at 125 °C, (b) at 150 °C, (c) at 175 °C and (d) at 225 °C.

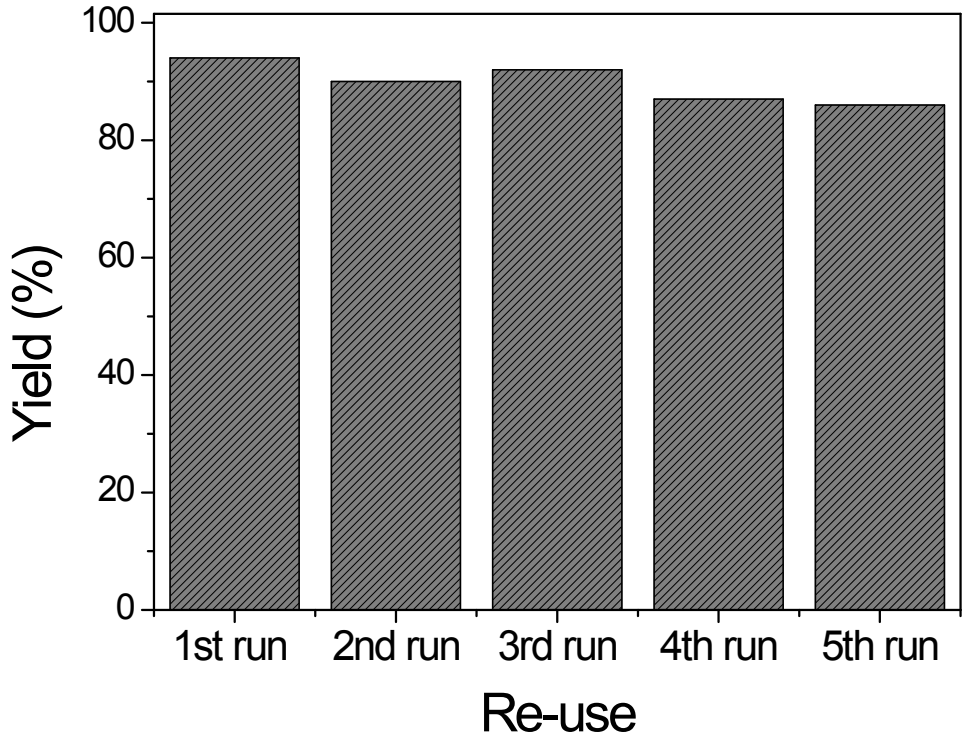

Fig. S8 Re-usability test of the synthesized ZnO plate as heterogeneous catalyst for the synthesis of 5-phenyl-1H-tetrazole.

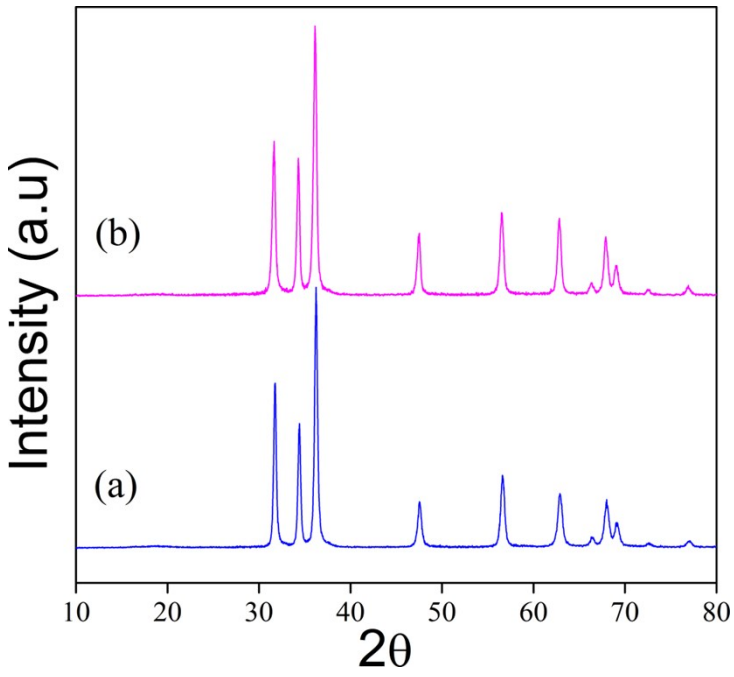

Fig. S9 XRD of (a) pristine and (b) reused (after 5th cycle) ZnO nanostructured materials.

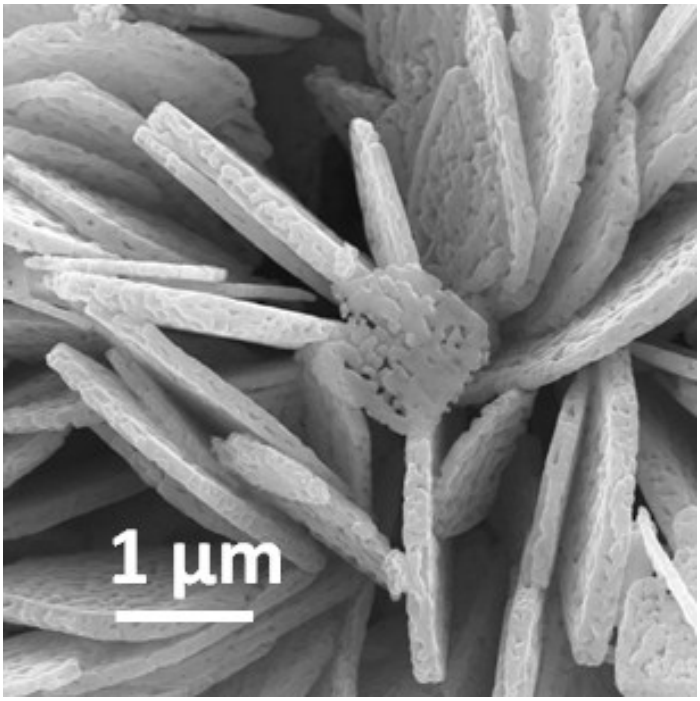

Fig. S10 SEM image of reused (after 5th cycle) ZnO nanostructured materials.

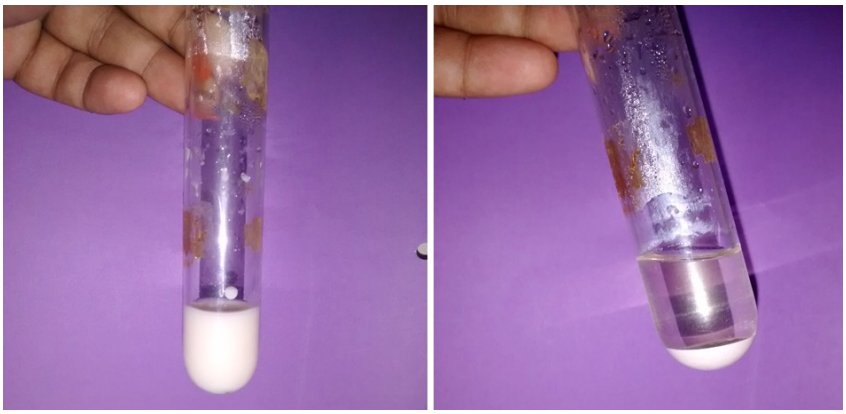

Fig. S11 Photographs of reaction vessel after reaction.

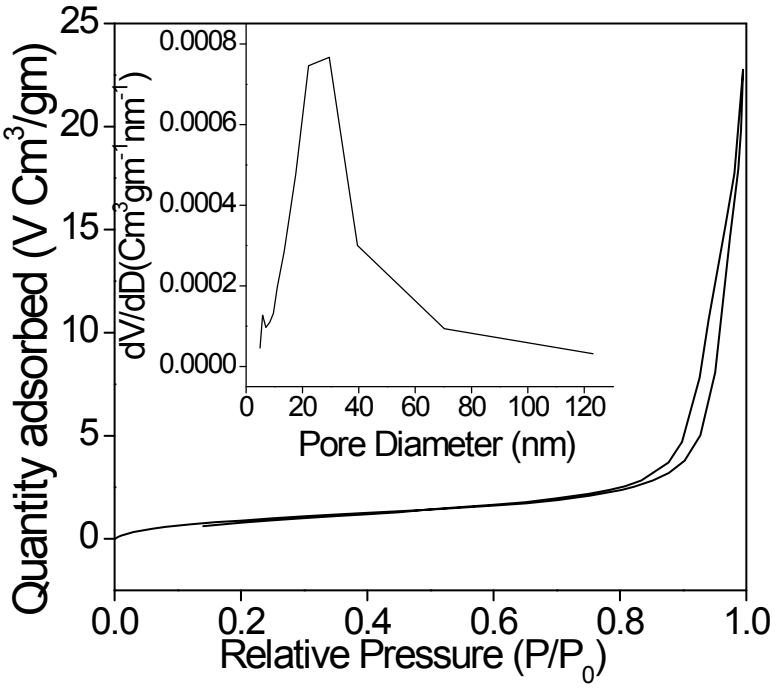

Fig. S12 Nitrogen sorption isotherm and corresponding pore size distribution (inset) curve of reused (after 5th cycle) ZnO nanostructured materials.

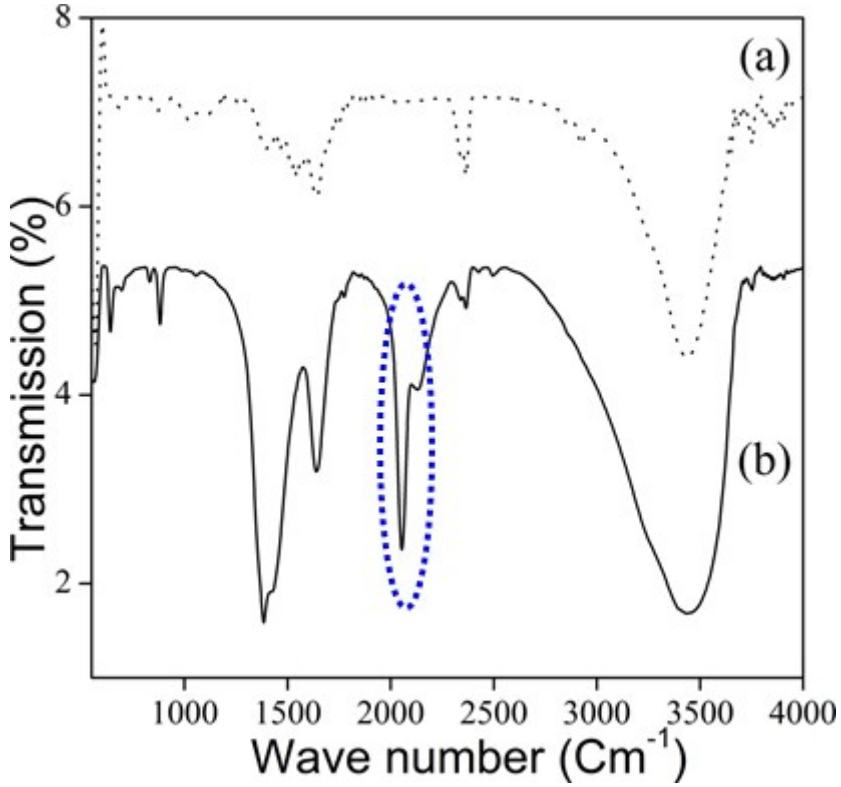

Fig. S13 FT-IR spectra of (a) pristine and (b) reused (after 5th cycle) ZnO nanostructured materials.

From the Fig. S8, it is evident that the catalyst is re-sable for at list 5 times. The yield of 5-phenyl-1H-tetrazoles is reduced from 94 to 86 % after consecutive reuse of synthesized nanostructured ZnO as heterogeneous catalyst. However the reduction of 8%, after 5th cycle, is very nominal. To find the origin of the reduction of catalytic activity, we have fully characterized the re-used catalyst by XRD (Fig S9), FE-SEM (Fig S10). We did not find any distinct structural and morphological change. Further, we did not find any change in whiteness of pristine and reuse catalyst and thus the probability of coke formation can be ruled out Fig. S11. However, in the N_2 sorption study (Fig S12) and FT-IR spectroscopic analysis of re-used catalyst (Fig S13) some distinct change was observed. Although no distinct change in sorption isotherm was observed, but a distinct decrease in total surface area and pore volume was observed. Further in FT-IR spectrum, presence of additional band for CN group (the blue circled band) indicate the existence of nitrile group even after washing with acetone. Probably, these nitrile groups bind with the active site of catalyst, reduced total surface area and *in-turn*, reduced the catalytic activity.

Table S1. Variation of crystallite size and surface area with calcination temperature of the synthesized 3D assembled porous ZnO plates.

Sample	**Crystallite Size (nm)**	**Pore Volume (cm^3/gm)**	**Surface area (cm^2/g)**
ZnO-400	14	0.2674	24
ZnO-500	18	0.3338	15
ZnO-600	24	0.3366	8

Table S2. A comparison of the heterogeneously catalyzed synthesis of 5-phenyl-1-H tetrazole form benzonitrile and NaN_3 reported in literature with the present hierarchically assembled porous rectangular ZnO Nanoplates towards flower.

Entry	Catalyst	NaN_3[a] (mmol)	Temp. (°C)	Time (h)	Yield (%)	Ref.
1.	**ZnO Plate**	**1.1**	**125**	**14**	**94**	**Present work**
2.	3D Porous ZnO	1.1	125	14	87	[3]
3.	Bulk ZnO	1.1	125	14	51	-------
4.	ZnO microtubes	1.1	125	14	92	[4]
5.	ZnO nanoparticles	1.1	120	14	72	[5]
6.	Mesoporous ZnS	2	120	36	84	[6]
	HNO_3 activated Mesoporous ZnS			12	60	
				36	96	
7.	CoY Zeolite	2	120	14	90	[7]
8.	Zn/Al hydrotalcite	1.5	120	12	84	[8]
9.	Zinc Hydroxyapatite	2	120	12	78	[9]
10.	$FeCl_3$–SiO_2	1.5	120	12	79	[10]

[a.] with respect to 1 mmol benzonitrile

Entry 2 The Bulk ZnO (commercial) which we have used as zinc source for 3D Porous ZnO structure.

Entry 4 Nano ZnO was employed for the reaction 72 % yield of 5-benzyl-1-H tetrazole was obtained which less than the present work.

Entry 5 84 % yield was observed in 36h of reaction time over mesoporous ZnS. Whereas 96% yield was observed in same tine over HNO_3 mesoporous ZnS, but only 60 yield was observed in 12 h of reaction time with the HNO_3 mesoporous ZnS.

However, in all the cases they used excess amount of NaN_3.

Entry 6 90% yield was obtain, but excess amount of NaN_3 was used.

Entry7 Comparable yield was observed with higher amount of NaN_3.

Entry 8 Lower yield was observed with higher amount of NaN_3.

Entry 9 Lower yield was observed with higher amount of NaN_3 and catalyst.

NMR, IR and CHNS data of the synthesized tetrazole.

2-(1H-tetrazol-5-yl) pyridine

2-(1-H-Tetrazole-5-yl) pyridine: White solid; **FTIR (KBr, cm^{-1}):** 3455, 2935, 2416, 1465, 1172, 1027, 1065, 804, 749. **^{1}H NMR (200 MHz, DMSO-*d*$_6$)[11]:** δ 8.81 (d, J = 4.0 Hz, 1H), 8.25 (d, J = 8.0 Hz, 1H), 8.14-8.06 (m, 1H), 7.68-7.62 (m, 1H); **^{13}C NMR (200 MHz, DMSO-*d*$_6$):** δ 157.96, 149.7, 143.32, 137.87, 125.71, 122.21; *m/z* calculated for $C_6H_5N_5$ $[M+H]^+$ 147.0472, found 147.0472

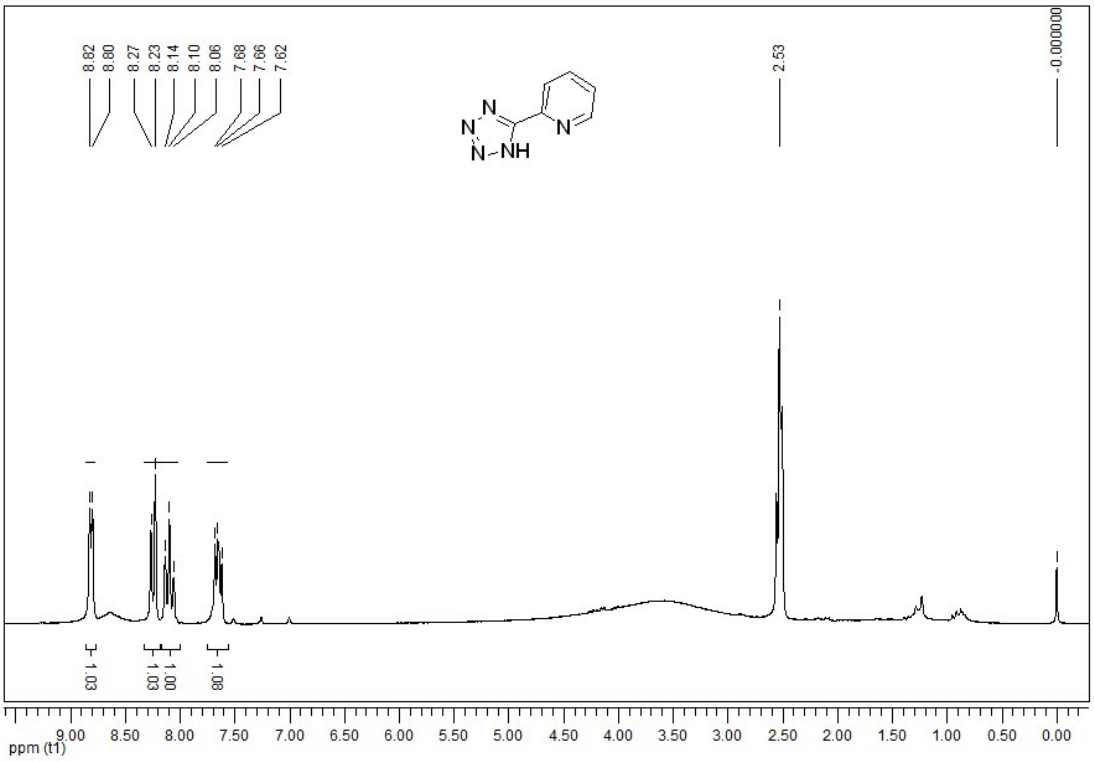

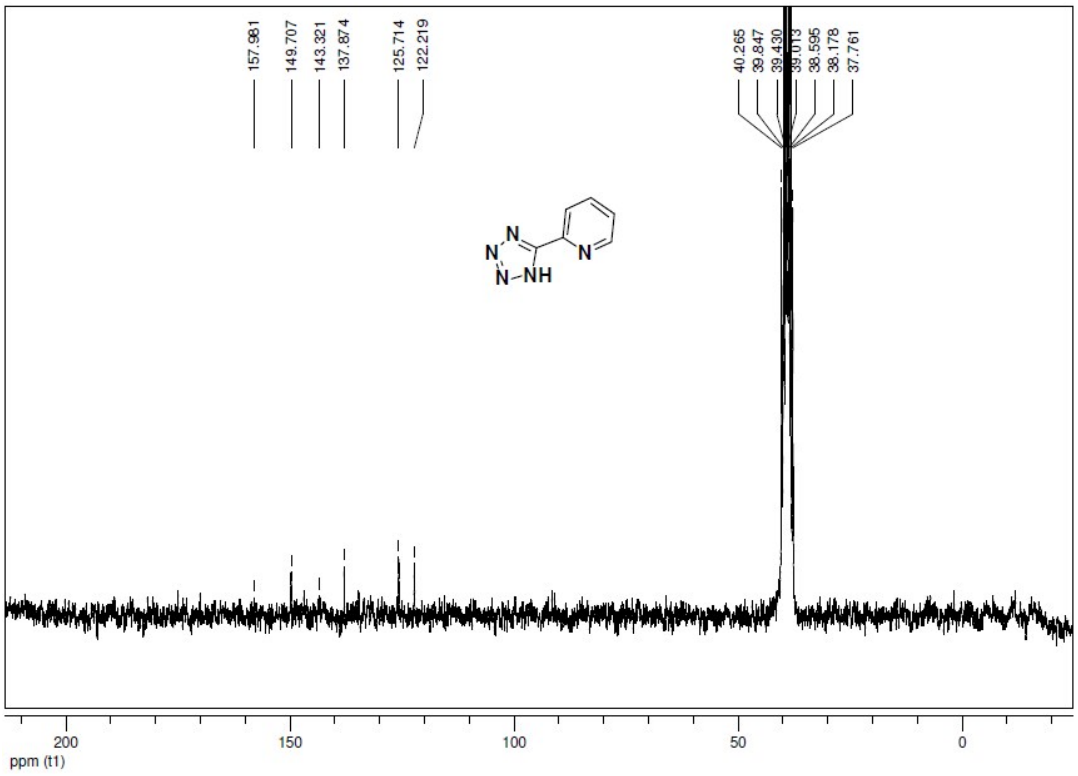

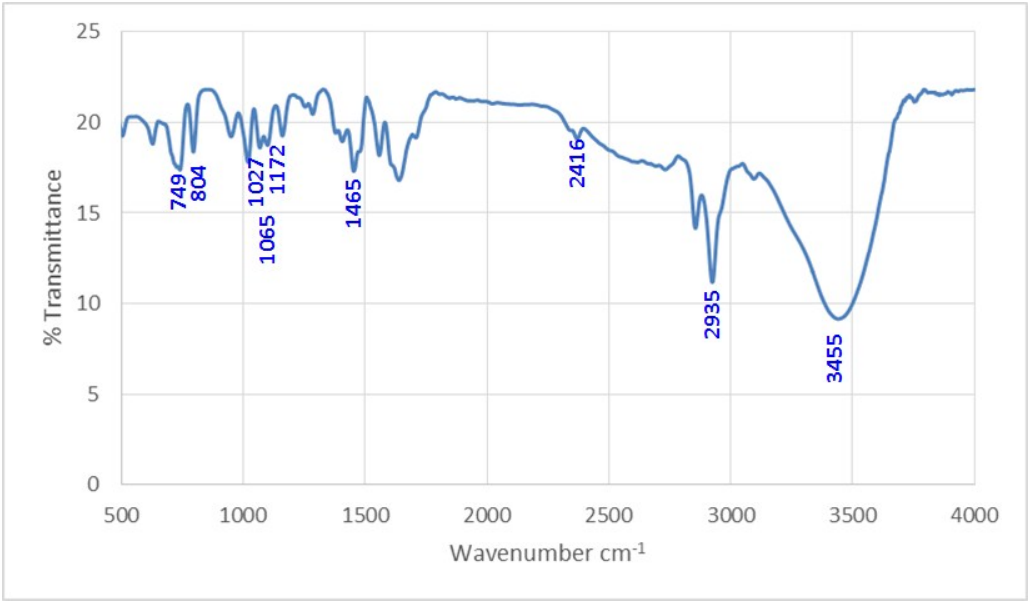

4-(1H-tetrazol-5-yl) phenol

4-(1H-tetrazol-5-yl) phenol: Greyish White solid; FTIR (KBr, cm^{-1}): 3380, 2646, 2399, 2259, 1615, 1512, 1419, 1283, 1184, 1088, 843, 645. **^{1}H NMR (200 MHz, DMSO-*d*$_6$) [11]:** δ 10.18 (broad s, 1H), 7.87 (d, J = 8.2 Hz, 2H); 6.95 (d, J = 8.0 Hz, 2H); **^{13}C NMR (200 MHz, DMSO-*d*$_6$):** δ 159.96, 155.88, 128.75, 116.13, 114.74; *m/z* calculated for $C_7H_6N_4O$ $[M+H]^+$ 163.0614, found 163.0613.

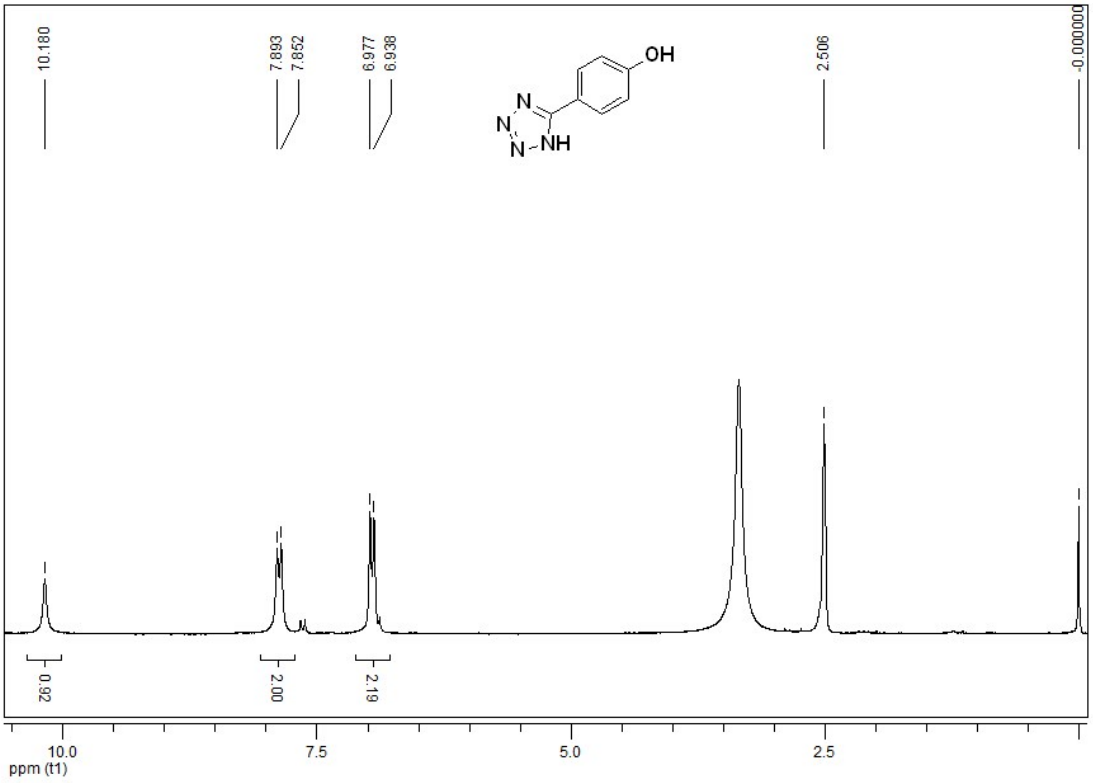
10.180
7.893
7.852
6.977
6.938
2.506
-0.000000
OH
N
N
N
NH
0.92
2.00
2.19
10.0
7.5
5.0
2.5
ppm (t1)

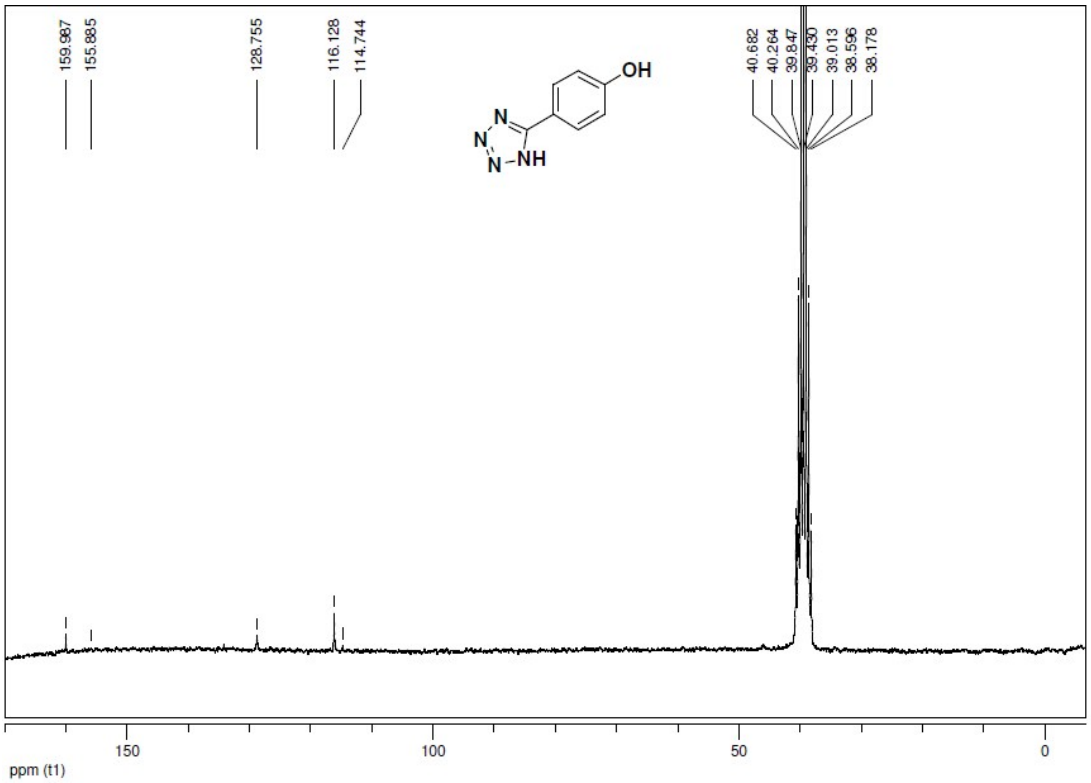
159.987
155.885
128.755
116.128
114.744
40.682
40.264
39.847
39.430
39.013
38.596
38.178
OH
N
N
N
NH
150
100
50
0
ppm (t1)

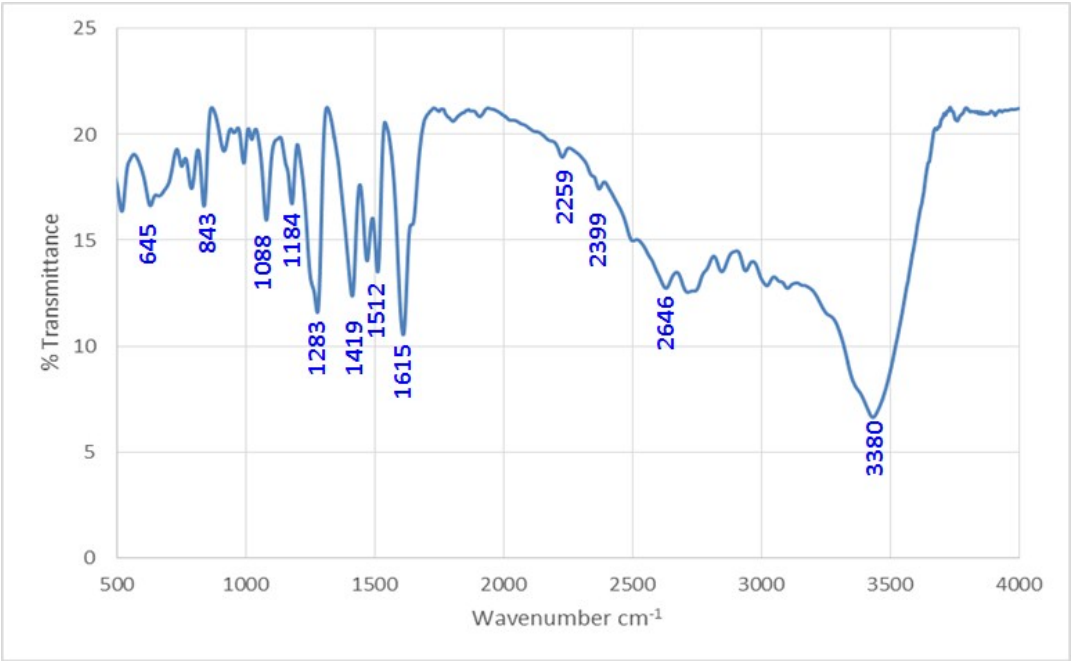

5-benzyl-1H-tetrazole

4-(1H-Tetrazole-5-yl) benzonitrile: White solid; FTIR (KBr, cm^{-1}): 3100, 2384 1547, 1258, 1078, 903, 703. **^{1}H NMR (200 MHz, DMSO-*d6*) [12]:** δ 7.36-7.31 (m, 2H), 7.28-7.26 (m, 3H), 4.29 (s, 2H); **^{13}C NMR (200 MHz, DMSO-*d6*)** δ 155.17, 135.86, 128.61, 128.55, 126.89, 28.81. *m/z* calculated for C8H8N4 $[M+H]^{+}$: 161.0822, found 161.0829.

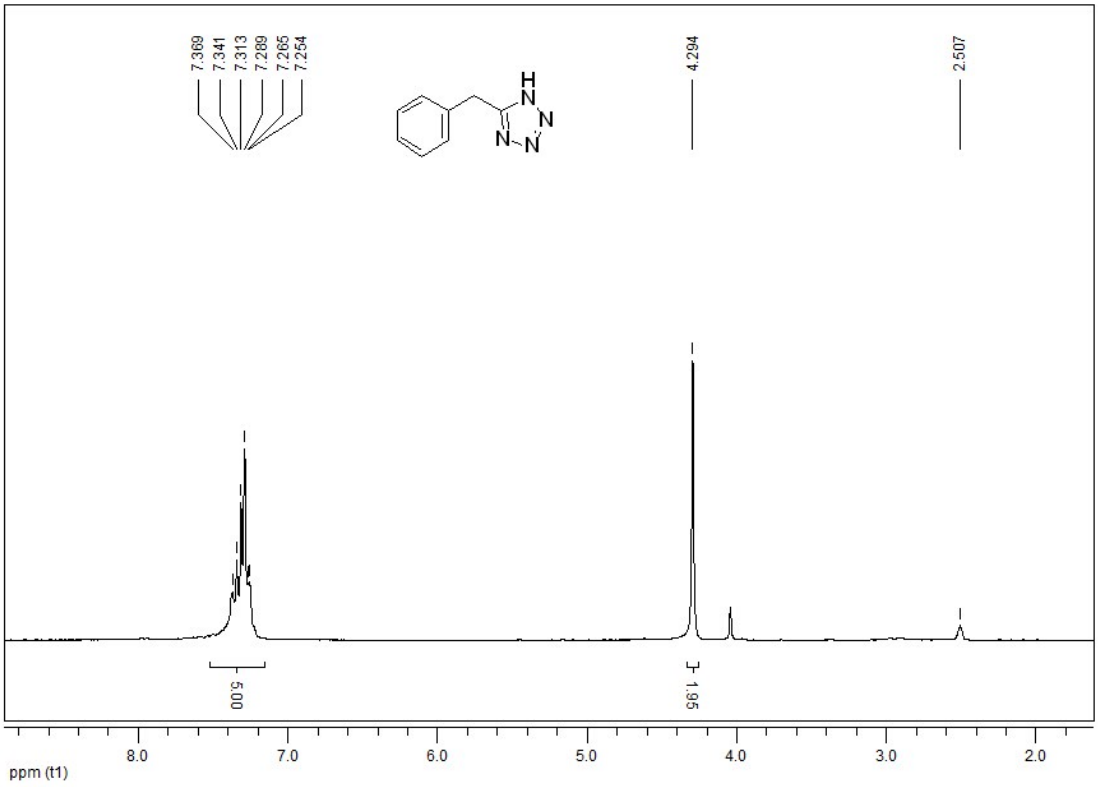

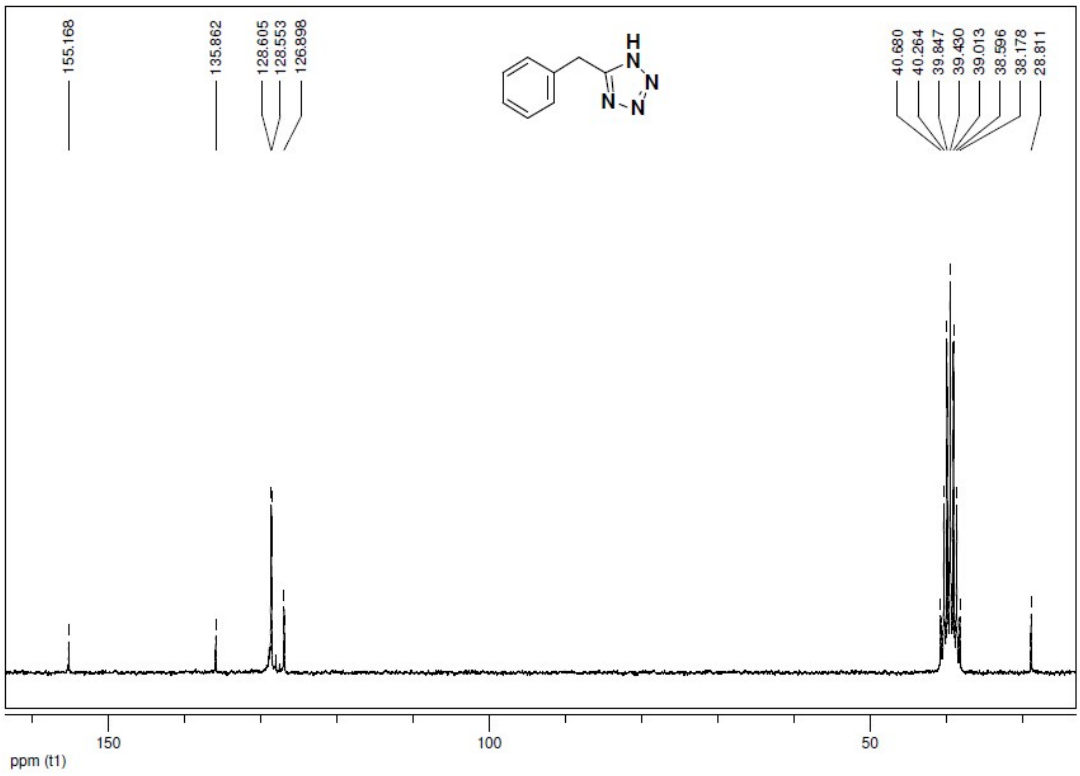

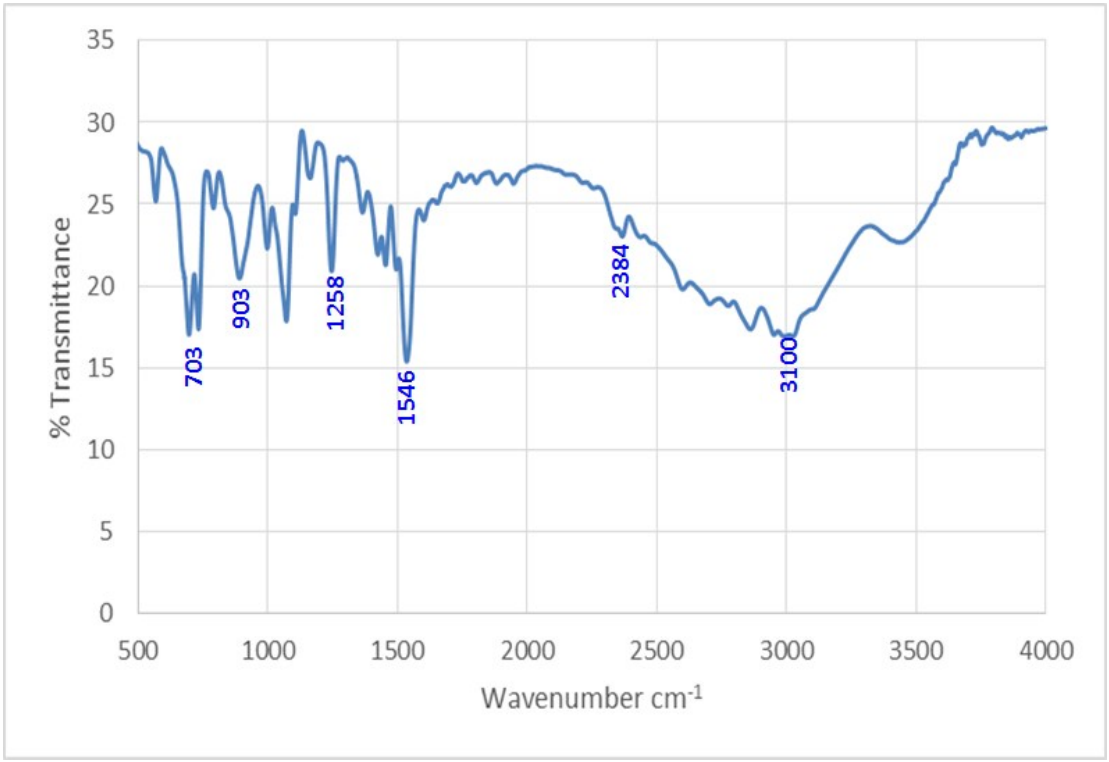

4-(1H-tetrazol-5-yl) pyridine

4-(1-H-Tetrazole-5-yl) pyridine: White solid; FTIR (KBr, cm^{-1}): 3477, 2942, 2832, 2380, 1644, 1539, 1439, 1107, 854. **^{1}H NMR (DMSO-d6, 200 MHz) d ppm ^{13}:** 8.03 (d, J = 4 Hz, 2H), 8.82 (d, J = 4 Hz, 2H). **^{13}C NMR (DMSO-d6, 200 MHz) d ppm:** 155.01, 149.75, 132.93, 120.49. m/z = 147, 119, 92, 78, 62, 50.

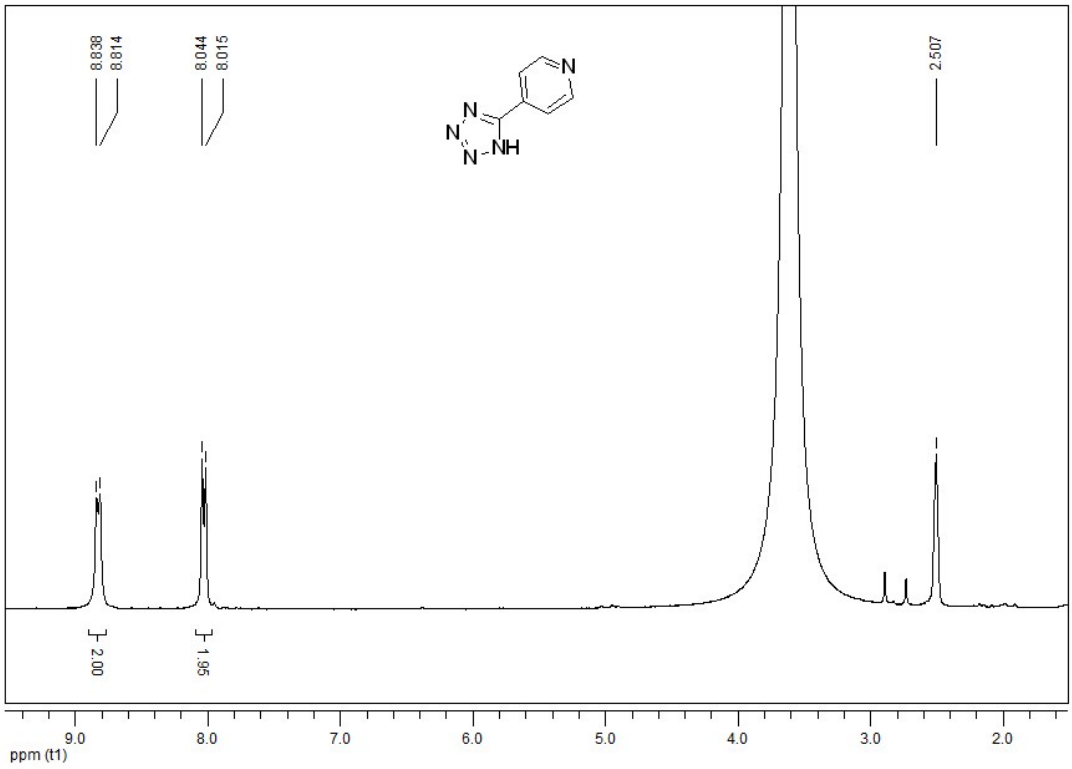
8.838
8.814
8.044
8.015
2.507
2.00
1.95
9.0
8.0
7.0
6.0
5.0
4.0
3.0
2.0
ppm (t1)

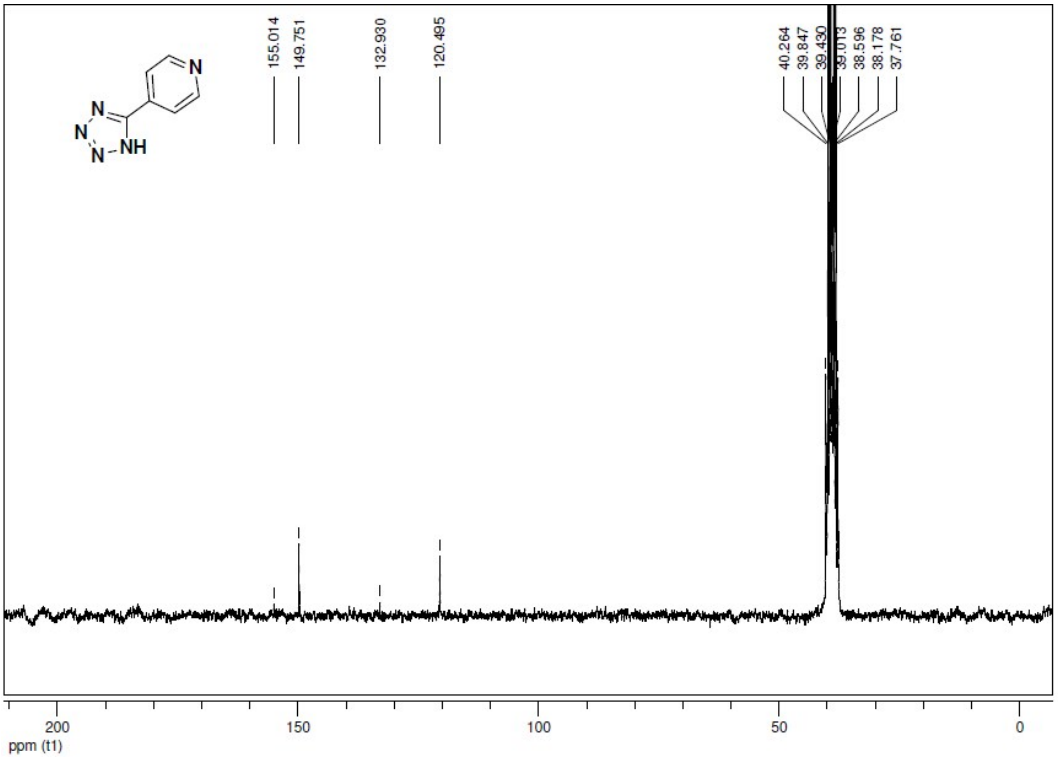
155.014
149.751
132.930
120.495
40.264
39.847
39.430
39.013
38.596
38.178
37.761
200
150
100
50
0
ppm (t1)

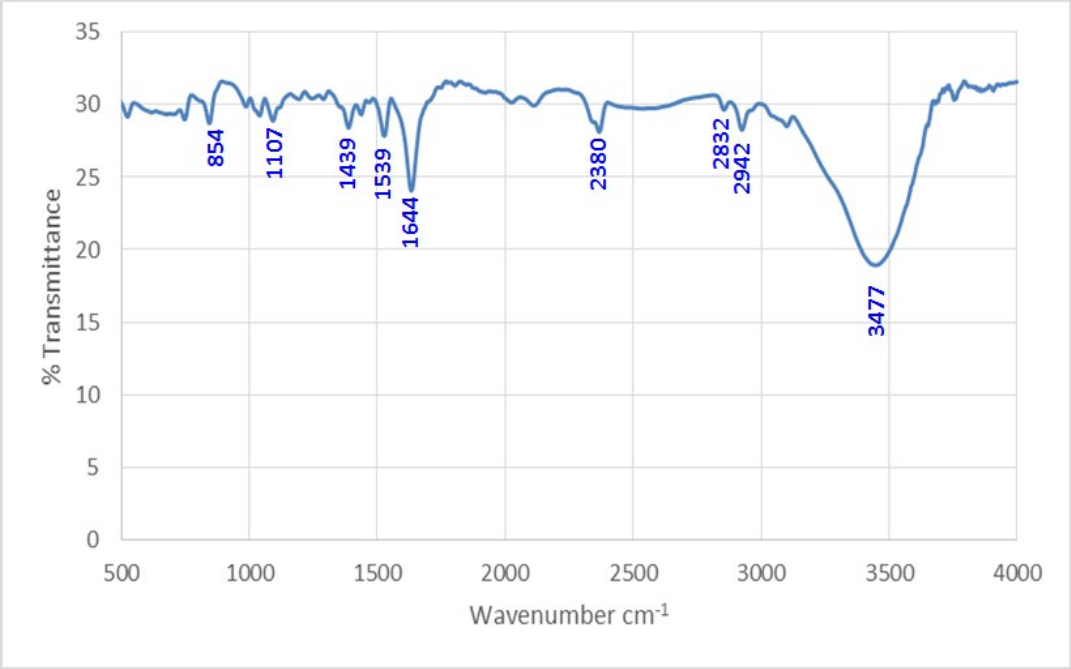

4-(1H-tetrazol-5-yl) benzaldehyde

4-(1H-Tetrazole-5-yl) benzaldehyde: White solid; FTIR (KBr, cm_1): 3442, 2649, 1682, 1307, 1216, 996, 844. **^{1}H NMR (DMSO-d$_6$, 200 MHz) d ppm:** 8.13 (d, J = 8.2 Hz, 2H), 8.27 (d, J = 8.2 Hz, 2H), 10.1 (s, 1H). **^{13}C NMR (DMSO-d$_6$, 200 MHz) d ppm ^{13}:** 192.18, 155.06, 139.21, 137.04, 129.85, 127.07. m/z = 174, 146, 130, 116, 102, 90, 57, 43.

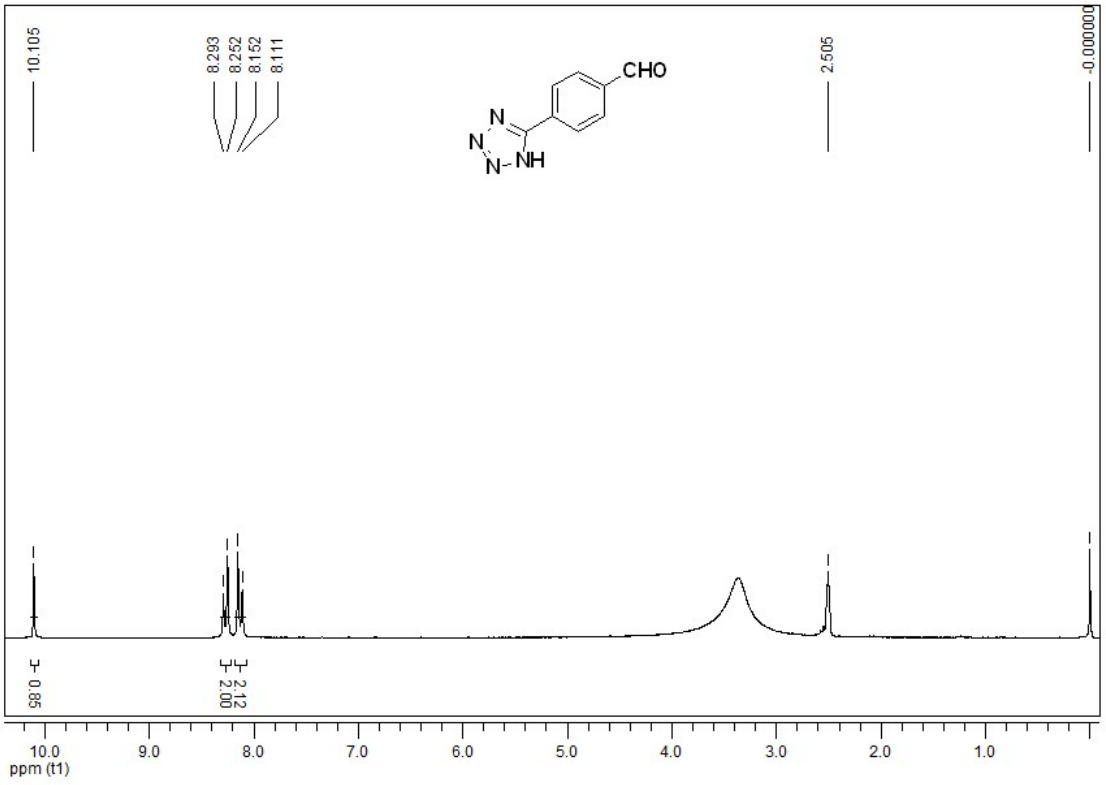

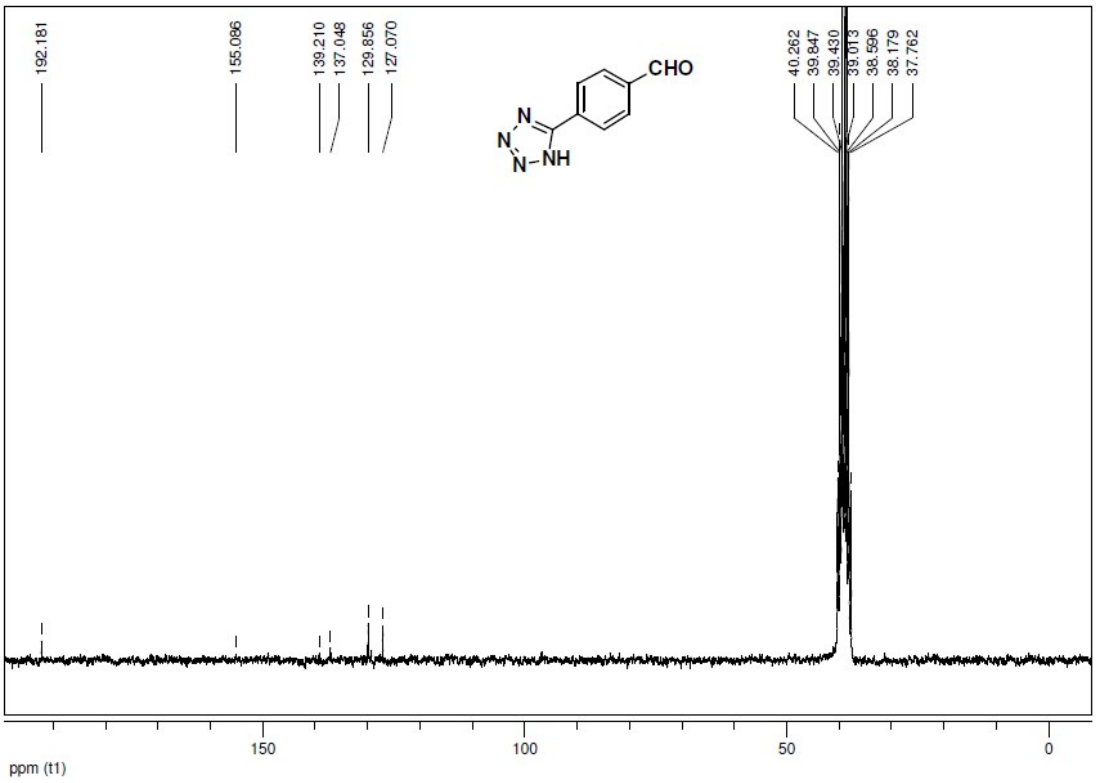

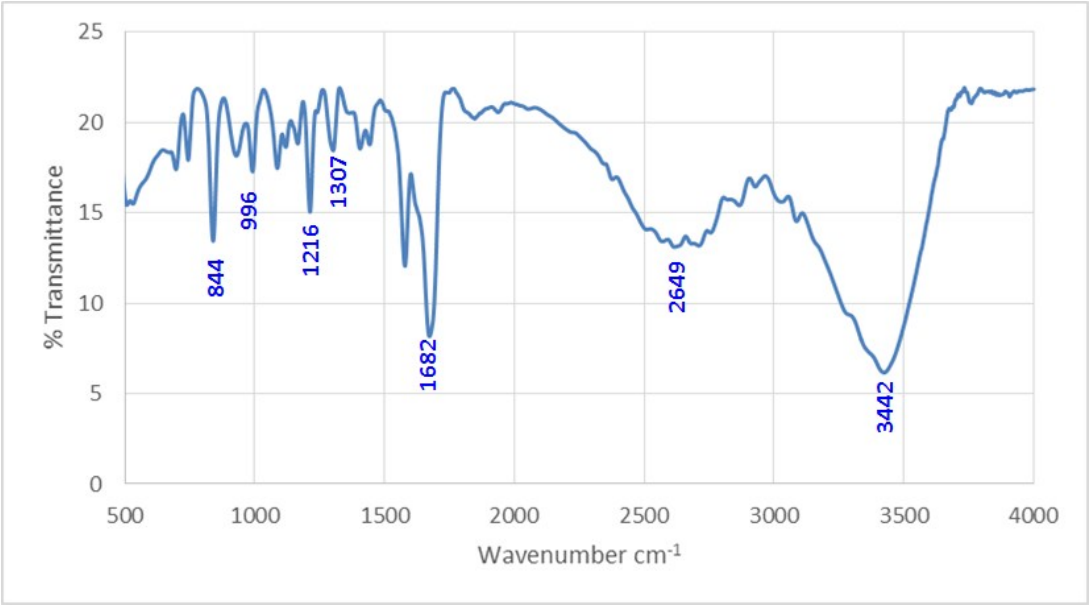

2-(1H-tetrazol-5-yl) benzonitrile

4-(1H-Tetrazole-5-yl) benzonitrile: White solid; FTIR (KBr, cm^{-1}): 3467, 2933, 2372, 2233, 1659, 1412, 1170, 782. **^{1}H NMR (DMSO-d6, 200 MHz) d ppm ^{13}:** 8.07 (m, 2H), 7.76 (m, J = 7.8 Hz, 1H), 7.94 (m, 1H) **^{13}C NMR (DMSO-d6, 200 MHz) d ppm:** 155.52, 134.94, 133.82, 131.40, 129.7, 127.59, 117.26, 110.22 and 15.54 m/z = 171, 143, 129, 103, 62.

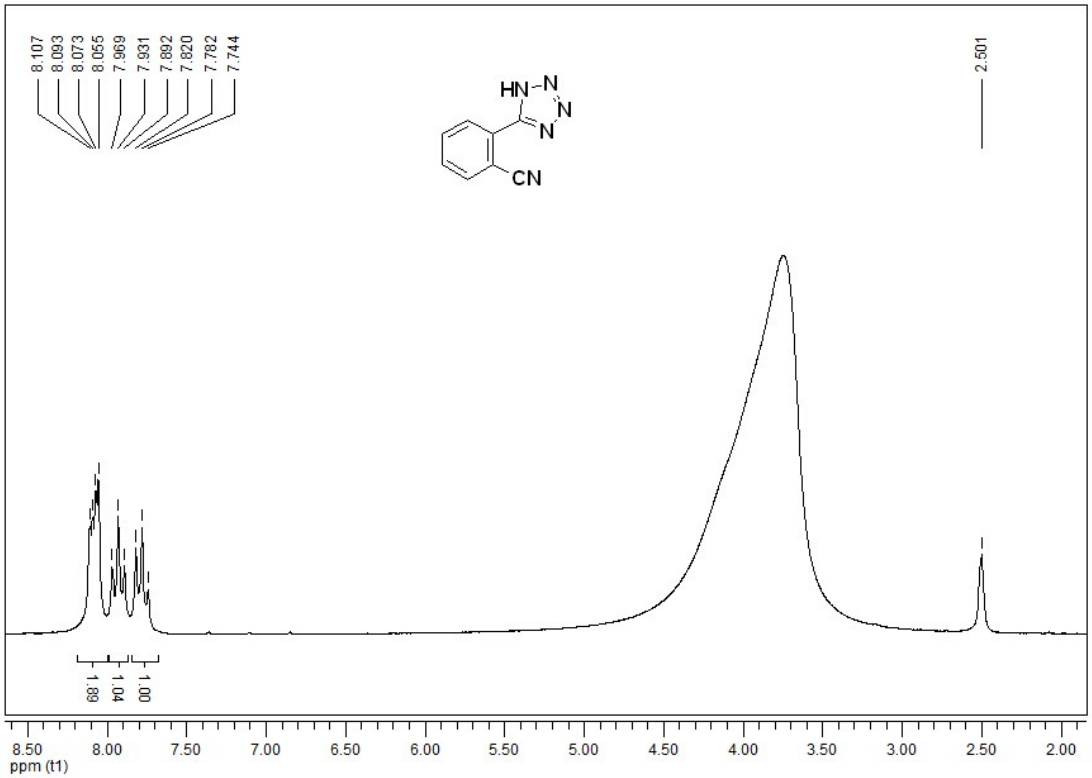
8.107
8.093
8.073
8.055
7.969
7.931
7.892
7.820
7.782
7.744
2.501
HN
N
N
N
CN
1.89
1.04
1.00
8.50
8.00
7.50
7.00
6.50
6.00
5.50
5.00
4.50
4.00
3.50
3.00
2.50
2.00
ppm (t1)

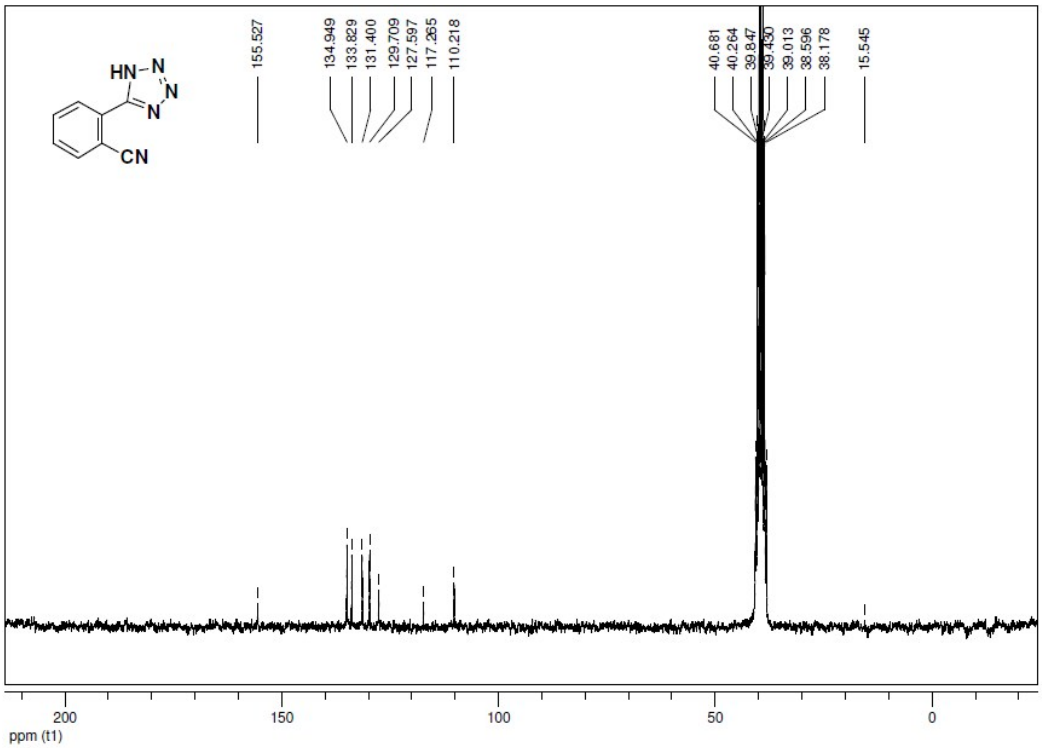
HN
N
N
N
CN
155.527
134.949
133.829
131.400
129.709
127.597
117.265
110.218
40.681
40.264
39.847
39.430
39.013
38.596
38.178
15.545
200
150
100
50
0
ppm (t1)

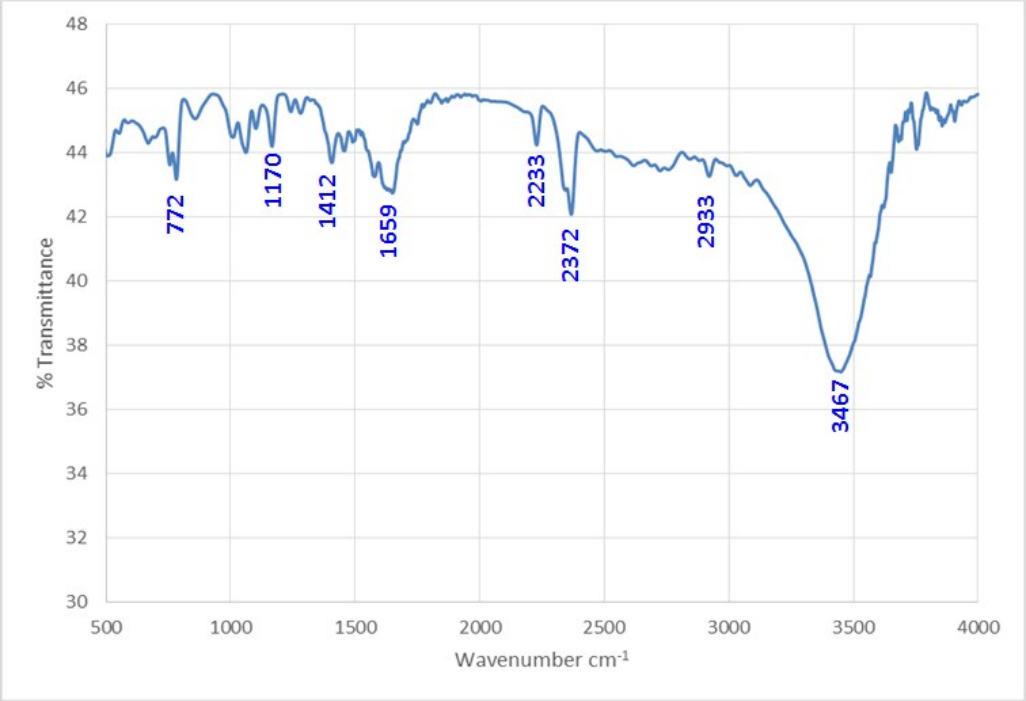

References.

1. A. Sutkaa, J. Zavickisb, G. Mezinskisa, D. Jakovlevsc and J. Barloti, *Sensors and Actuators B*, 2013, **176** 330.
2. K. Arshak and I. Gaidan, *Thin Solid Films* 2006 **495** 286.
3. A. Sinhamahapatra, A. K. Giri, P. Pal, S. K. Pahari, H. C. Bajaj, A. B. Panda, *J. Mater. Chem*. 2012, **22**, 17227-17235.
4. A. K. Giri, A. Sinhamahapatra, S. Prakash, J. Chaudhari, V. K. Shahi, A. B. Panda, *J. Mater. Chem. A*. 2013, **1**, 814-822.
5. M. L. Kantam, K. B. Shiva Kumar, C. Sridhar, *Adv. Synth. Catal.* 2005, **347,** 1212-1214.
6. L. Lang, B. Li, W. Liu, L. Jiang, Z. Xu, G. Yin, *Chem. Commun.* 2010, **46**, 448-450.
7. V. Rama, K. Kanagaraj, K. Pitchumani, *J. Org. Chem.* 2011, **76**, 9090-9095.
8. M. L. Kantam, K. B. Shiva Kumar, K. P. Raja, *J. Mol. Catal. A: Chem.* 2006, **247**, 186-188.
9. M. L. Kantam, V. Balasubrahmanyam, K. B. S. Kumar, *Syn. Commun.* 2006, **36,** 1809-1814.
10. M. Nasrollahzadeh, Y. Bayat, D. Habibi, S. Moshaee, *Tetrahedron Lett.* 2009, **50**, 4435-4438.
11. Z. P. Demko and K. B. Sharpless, *J. Org. Chem.,* **2001**, *66*, 7945.

12. D. Amantini, R. Belaggia, F. Fringuelli, F. Pizzo and L. Vaccaro, *J. Org. Chem.* **2004**, *69*, 2896
13. A. Teimouri and A. N. Chermahini, Polyhedron, **2011,** 30, 2606.